MEASUREMENT OF THERMAL WAKES IN COMPRESSOR SECONDARY AIR SYSTEMS USING LOW FREQUENCY THERMOCOUPLE DATA

Mark Puttock
Thermo-Fluid Mechanics Research Centre
University of Sussex
M.Puttock@sussex.ac.uk

Prof. Martin Rose
Thermo-Fluid Mechanics Research Centre
University of Sussex
M.G.Rose@sussex.ac.uk

ABSTRACT

Experimental temperature measurements are made using two Datatel radio telemetry systems with K-type glass insulated thermocouples inside the Sussex Multiple Cavity Rig (MCR). Currently the MCR supports independent rotational control of both the rotor (disc pack) and a central shaft. The results presented here highlight a novel application whereby the wakes of a set of rotating blocks are captured whilst the rig is at full speed using low frequency data acquisition. This takes advantage of the relative motion of the two telemetry systems to look at flow structures that are usually outside of the frequency domain of the instrumentation.

INTRODUCTION

The Sussex MCR was developed as part of the IGAS-GT European Commission Projects to investigate steady heat transfer of secondary air systems inside HPC drum cavities. The prediction of which is a contributing factor in the overall design of aero-engines, as it has a significant effect on compressor blade clearances. The MCR features engine representative titanium alloy with 82 thermocouples spread over 3 discs. The throughflow air enters and leaves through an annular space defined by the disc bore and central shaft. The central shaft is driven in a co- or counter-rotating fashion with respect to the rotor and features 36 surface and air thermocouples spaced at 9 axial locations. The shroud temperature of the rotor is driven by a radiant heater array, which drives natural convection inside the cavities.

To match the exit conditions of the bore flow a set of 6 rectangular blocks were installed to restrict the annular area at inlet and induce engine representative swirl, this component is fixed to the rotor stub-shaft downsteam of the main bearing. There is a 0.5mm gap between the central shaft and inner radius of the blocks, with all rotating instrumentation upstream. As the central shaft and rotor are free to rotate relative to one another the protruding air thermocouples would pass through any blade (block) wakes in the bore flow.

Whilst buoyancy-induced flow structures present in a rotating cavity are not discussed in this paper the reader is referred to a review by (Owen 2015) . Further works conducted previously on the MCR with axial throughflow are detailed in: (Alexiou 2000), (Miché 2008), (Long 2007) and (C. M. Long 2007)

EXPERIMENTAL FACILITY

The rotating disc pack is manufactured from Ti-6Al-4V titanium alloy and supported via two bearings; the rear grease packed and the forward an oil-fed axial-roller bearing from a Rolls-Royce IP turbine. The inner-race is bolted to the stub-shaft of the rotating assembly with a continuous oil circulation provided which also removes any entrained air. The axial-rollers are contained in a cage that is fixed to the outer casing, which made from 15mm thick mild steel. The radiant heater array, to simulate the temperature of the HP Compressor main flow, is fixed to the outer casing leaving a small radial gap.

The bore axial through-flow is driven by an Atlas Copco Screw Compressor with a manual control bypass valve. This passes through an Atlas Copco air dryer to ensure there is no entrained vapour passing to the test section. The mass flow rate is measured via an in-house developed and calibrated Venturi section, a differential pressure measurement gives a calibrated voltage output that is recorded using an NI PXI-6659, connected via an SCB-68 terminal block. The total temperature is recorded using a K-type thermocouple connected to an Agilent 34970A, which is used for all stationary temperature measurements.

The rotational speed of the rotor assembly and shaft are measured using magnetic pickup probes, outputting an analogue voltage, connected to the NI-PXI6659. Labview routines are used to detect the frequency and convert into an rpm for rig monitoring.

Adjustment of rig pressure is via a butterfly valve at the exhaust, this allows fine control of the mass flow to within 1% of set test conditions. The bore flow is introduced to the test section via two

1

30mm pipes into a small annular plenum at the six and twelve o'clock positions in the circumferential direction. The flow moves radially inward and into the axial direction via twelve 24mm diameter holes that pass through both the inner-radius of the annular plenum and the stationary component of the shaft assembly.
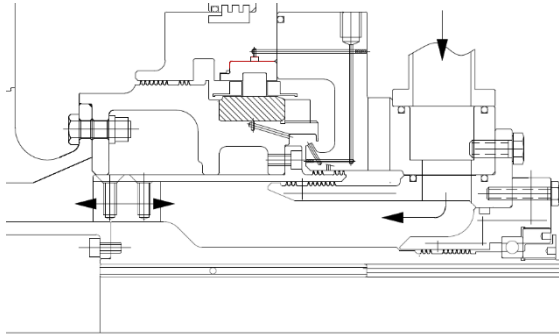
Figure 1: Schematic of MCR inlet

The inlet region of the test section features two labyrinth seals; the smaller is between the stationary and rotating shaft components whilst the larger is the between the stationary shaft component and rotating section attached to the stub-shaft of the rotor assembly. The total temperature at inlet is measured at two locations 180° apart protruding into the inlet from the stationary shaft mount; again K-type thermocouples are used. The labyrinth seals are pressure balanced to ensure that the bore flow path is sufficiently sealed and that there is no leakage of oil from the axial-roller bearing. The cold-build clearances are of the order 0.1mm with the labyrinth seal pressure differential manually balanced to ±10mbar throughout testing through actuated proportional valve. The balancing air is fed from an auxiliary supply.

SHAFT INSTRUMENTATION

Glass fibre K-type insulated thermocouple wire is used for all Shaft thermocouples, in total 36 are arranged in 4 circumferential rows (2 surface mounted and 2 air) with 9 axial locations each. The air thermocouple protrude 4mm from the surface of the shaft and are unsupported. Continual monitoring during the current testing program has shown that they do not change position significantly.

A Datatel radio telemetry system is used to record the rotating thermocouples, the system comprises of a master and 2 extension modules connected in a serial bus. The thermocouples signals are sampled sequentially with a delay of 390 micro-seconds between each channel and averaged over 8 cycles before data transmission. The resultant sampling frequency in 3Hz. Each of the modules has an on-board Platinum Resistance Thermometer (PRT) for a cold junction reference

developed and calibrated in-house. Rotating frame cold junction compensation uncertainty is within ±0.1K.

The calibration procedure for all thermocouples and PRTs used in the current setup are detailed in (Atkins 2014).

Given the current setup of the telemetry system, system drift cannot be considered normal is distribution and as such the error sources are added to give a worst case combined uncertainty of approximately ±0.5K. Since errors are assumed to not be normal, there is no reduction in uncertainty through averaging, (Atkins 2014). A more detailed assessment of errors present in the MCR rig is given by (Long 2007).

ROTOR INSTRUMENTATION

The rotating assembly is instrumented with 86 thermocouples which are peened into the surface of the titanium discs. Each thermocouple is routed circumferentially along an isotherm for a least 10 wire diameters to ensure that the bead itself is measured, by reducing the conduction errors.

An additional 92 channel Datatel radio telemetry system is used to transmit the data from the rotating assembly, comprising a master and 5 extension modules connected in a serial bus. A similar cold-junction compensation to the shaft instrumentation is used, as well as calibration procedure. The recording frequency is again 3Hz.

RESULTS AND DISCUSSION

At full rig operating speed the rotor and shaft rotate at approximately 8000 rpm, it is noted during testing that the rotor tends to decrease speed at average of 1 rpm every 5 minutes. As the rotor and shaft are not directly coupled but free to rotate relative to one-another there is generally a slip between them, indeed the windage due to the rotor tends to drives the shaft. During commissioning testing it has been noted that the shaft achieves a rotational speed of at least 250rpm without any motor drive. Whilst the rotor tends to have a smooth rpm profile, the shaft motor controller (an ABB ACS150) has to compensate for the windage resulting in an oscillation of 3-4 rpm that continues throughout a typical test cycle.

A rotational speed of 8000 rpm corresponds to approximately 133 Hz, taking into account the 6 flow blocks in the inlet region this results in a blade or 'block' passing frequency of 800Hz in the stationary frame. At this frequency level the currently used instrumentation is unable to resolve any unsteady flow structures in the bore flow path, this is also compounded by the stationary plenum which introduces the flow through 12 holes from the main supply.

As noted above there tends to be a relative slip between the shaft and rotor frames of reference,

given the windage effects and the resolution of both motor controllers this is typically of the order 20rpm. Even at this level the block passing frequency is 2Hz, whilst within the recording frequency of the instrumentation it does not satisfy the Nyquist criterion nor give sufficient time for the protruding thermocouples to fully respond. The typical spread in temperature reading from the first thermocouple downsteam from the block exit is shown in Figure 2, where the oscillation amplitude is 3.5K.
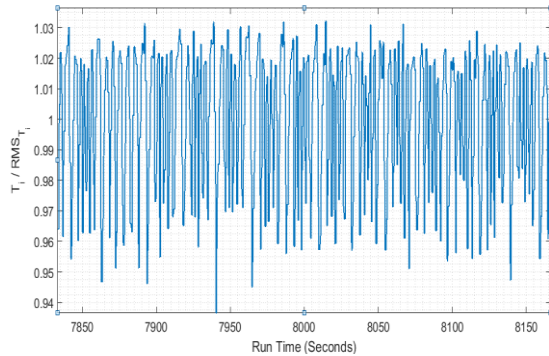
Figure 2: Temperature reading from first Thermocouple downsteam of block exit. The relative slip is approximately 26 rpm

With the gradual decrease in rotational slip between the two systems there is an eventual synchronization, with a period on both sides corresponding to a convergence and divergence. Once in sync the two systems tend to 'lock' together and will remain so for an extended period of time (this has been observed to last up to 45 minutes), this however seems to be a function of a number of parameters and is unpredictable. With manual modification of the motor controller settings it is possible to sync the two or engender a very low slip. The obvious advantage of this is that the block passing frequency can be reduced to such an extent that the thermal wakes can be visualized and recorded whilst satisfying the Nyquist requirements and the allowing the thermocouple sufficient time to respond to the gas temperature. It must however be stated that the recording of thermal wakes is a by-product of the current MCR setup and was never intended, as such the data presented is not anti-aliased. However the recorded data is the results of an 8-point averaging performed on-board the telemetry system, whilst not performing the same function as a low-pass filter it does help to mitigate the aliasing phenomenon. Regardless of the questions raised it still presents a novel measurement technique that is proving insightful to the behaviour of multiple cavity setups with axial throughflow.

SPACE-TIME DIAGRAMS

With knowledge of the rotational speeds of both shaft and rotor it is possible to calculate the relative slip and block passing frequency. Given the recording frequency of 3Hz the change in angular position of the blocks with respect to a shaft datum can be estimated and the number of full revolutions estimated via integration over a specified length of time. The presented data captures a syncing event during a standard test cycle, with both converging and diverging rpms. The bulk temperature of the rig was cooling down whilst still running at nominally full speed; this particular test cycle also showed an above average decrease in the rotor speed.
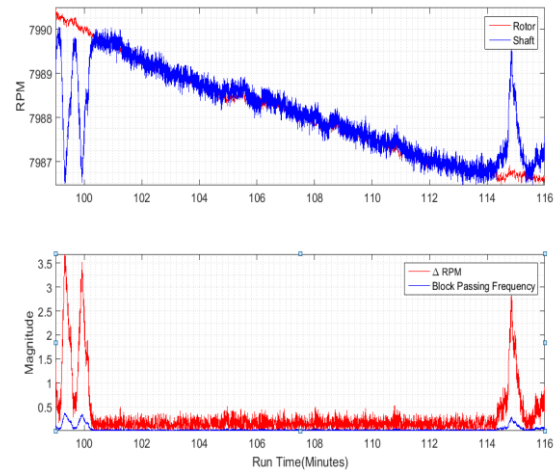
Figure 3: Rotor and Shaft speeds during test cycle (top). The resultant slip and block passing frequency are show below.

Figure 3 details the behaviour of the rotor and shaft during a 17 minute period. In the top graph the shaft is seen oscillating before the sync to compensate for windage, however once coupled to the rotor there are no fluid dynamic effects driving the shaft and it remains at the same rpm as the rotor. It is not until 114 minutes when the drop in the overall rotor speed has reached the same level as the lowest point of the initial shaft oscillation that they uncouple. At this point the shaft resumes its oscillatory behaviour, maintaining an average rpm of approximately 7988.5 rpm. It is interesting to note that the oscillation after the sync is of the same amplitude as before without the driving factor of rotor windage, suggesting that it is also a function of the motor control unit. It is worth noting that the observed amplitude of oscillation does tend to decrease when the shaft is rotating faster than the rotor.

The clear consequence of the oscillatory shaft behaviour is demonstrated in Figure 4. As the relative slip increases block passing frequency also increases leading to the period of each thermal wake being reduced, causing a tight grouping of wakes, as observed between 114.7 and 115.1 minutes. This is the motivation behind integrating the relative motion to calculate position as the speeds are not constant.

3
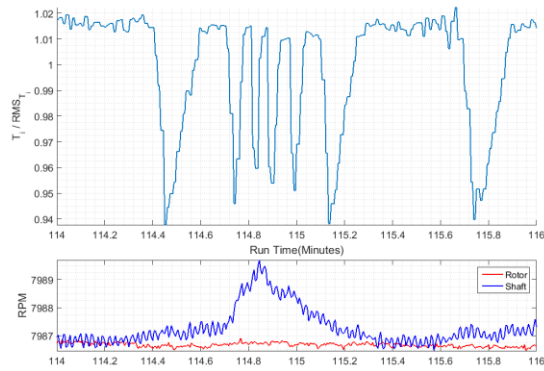
Figure 4: Effect of shaft oscillations on thermal wake period. First thermocouple downstream of block exit

Using the integral function to calculate relative position allows the time-base of the wake profile to become periodic. By dividing the instantaneous reading of each thermocouple by the root-mean-square (rms) value from the entire time shown in figure 2 (99-116 minutes) a space-time diagram can be generated to track the thermal wakes propagating along the bore path.
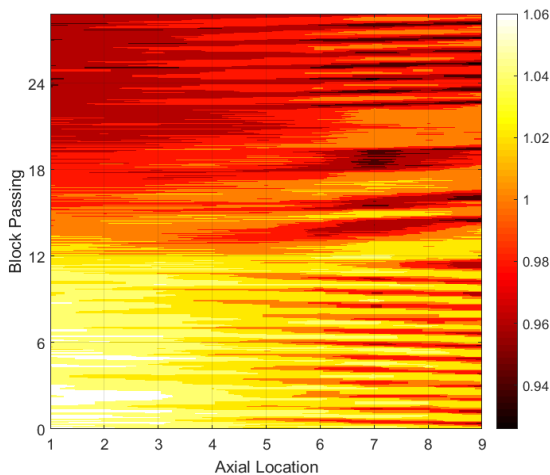
Figure 5: Space-Time diagram of Air Thermocouples along bore path. Location 9 is closest to block exit. Contours are of T_i / RMS_T

Figure 5 show the space-time diagram for all air thermocouples along the bore flow path. The integral method for calculating the block passing has proven remarkably accurate given the relatively crude measurement of rotational speed (a high speed digital encoder would allow direct calculation of relative position to a great accuracy). The number of high temperature regions near block exit (location 9, flow moves right to left) agrees with the number of block passing events, this is represented in multiples of 6 as this corresponds to complete relative rotations. Whilst there is strong agreement until 12 block passing events this does not continue when the shaft and rotor are in sync, this lasts for 14 minutes of run time but has been reduced in the temporal domain of Figure 5. The

integral counts continues to rise giving an estimated 9 block passing events, this is clearly in error as the variance of the contours show 4 high thermal regions, the error here can be accounted to the accuracy of the speed sensors. The magnetic pickup is operating at a 10 kHz and the monitoring software looks for a frequency in the waveform from which an rpm is deduced, whilst this is sufficient for the type of experimental work that has been traditionally been performed on the MCR it is not in this domain.

The contours of the block wakes show a strong signal until approximately location 4, located approximately 127 mm downstream of location 9. Also to note is the reversal of the wake gradient, suggesting that the wakes are travelling temporally backward, this can be attributed to the divergence of the relative speed and that the shaft is now rotating faster than the rotor. It is also apparent that the overall temperature is decreasing over time shown by the higher levels during the first 12 block passing and the later lower levels.
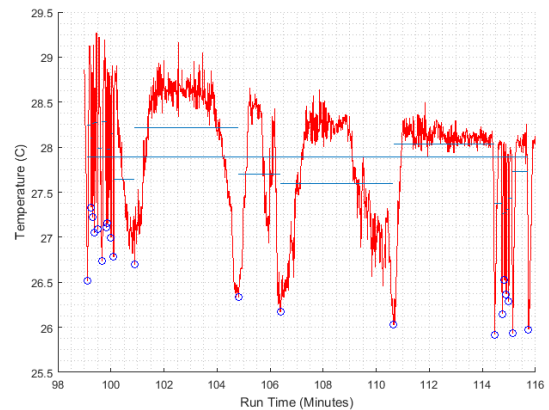
Figure 6: Location 9 air temperatures demonstrating rms skew.

As shown in figure 4 the varying level of slip leads to some of the events showing a long high temperature reading followed by a short low temperature dip, this leads to a skew when calculating the rms level as it is not periodic in time. Figure 5 demonstrates, for a single thermocouple closest to block exit, the effect of the skew on the data. Here the 'bulk' rms taken over the entire time period is drawn across the whole diagram, individual rms levels for single wakes are identified by smaller horizontal lines. The blue circles correspond to individual 'valleys' in the data, these are used to split each wake from its neighbour and compute a unique rms value. Whilst only showing a single thermocouple this is repeated for all axial locations, from which the space-time diagram can be reproduced.

With a unique rms level for each thermal wake and a periodic time base the data can be considered as an effective ensemble average as shown in Fig. 7. The thermal wakes can clearly be seen propagating the entire length of the test section in

this instance and the long term thermal transient removed from the contour map. It is expected that the low temperature wakes will dissipate however there a tentative suggestion of the effect of cavity ingestion of bore flow. Location 7 is positioned in the mid-plane of the first cavity after the block exit; this would suggest that any interaction of the wakes and cavity would most strongly be seen here. The relatively low levels between the wakes identified as dark regions would support the conjecture that the lower temperature fluid would stratify outwards into the cavity leaving the high temperature fluid in the bore and near shaft surface. Without high fidelity URANS calculations of both the block and cavities to gauge their interaction this is difficult to conclusively support from the presented data alone.
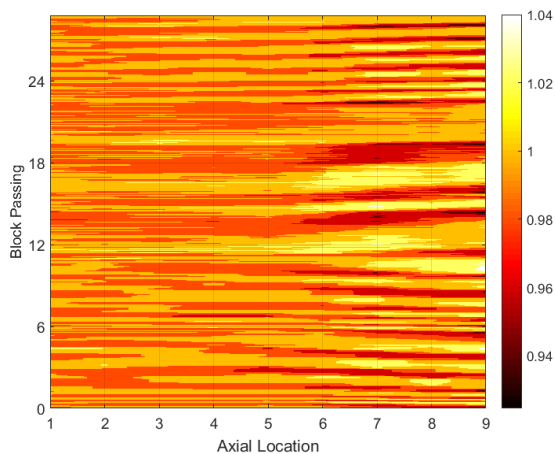
Figure 7: Ensemble averaged space-time of thermal wakes.

What can be estimated from the thermal wakes is the velocity of propagation in the bore flow; this can be compared to the velocity calculated from the mass flow rate. The difficulty here arises from the assumption of uniform flow across the annulus which is clearly not the case, to satisfy this a CFD calculation of the rig inlet region and blocks has been made.

NUMERICAL SETUP

To gain an approximate understanding of the flow fluid ANSYS CFX has been used to model the inlet plenum and transfer holes in the stationary frame and the rotating blocks. The flow domain is terminated at location 8 corresponding to the mid-line of the first cob. Numerical prediction of flow inside rotating cavities is still a very costly exercise and has not been attempted in this instance. The SST turbulence model is used as it gives more accurate prediction of flow separation under adverse pressure gradients which is clear from the outset.

An unstructured grid is used to model both stationary and rotating components with an automatic wall function as specified by CFX. Both domains total approximately 1.3 million elements,

with boundary layer inflation around all blocks. Given the nature of the bore delivery half an annulus has been calculated with periodic boundary conditions. A total pressure condition is used at inlet; a mass flow rate is set at outlet as there is no pressure instrumentation immediately downstream of the blocks and isothermal wall temperatures are used. Equation residuals were of the order 1e-6. Figure 8 shows an isometric view of the domain, the geometry has been simplified for ease of meshing with both labyrinth seals set as walls, given that the seals are balanced and the mass flow in or out is negligible.
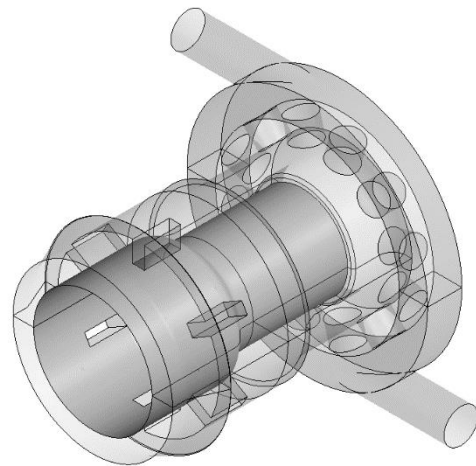
Figure 8: CFD domain used in calculation transformed to show full annulus. Darker surface is rotating shaft.

NUMERICAL RESULTS

The simulation has been run for two complete revolutions in 1 degree steps, corresponding to 720 steps in total. The following discussion is taken from the last time step as a great deal of information can be deduced without the need for averaging and the instantaneous nature of the flow structures can be observed.

Figure 9 shows streamlines through the flow domain, the disjointed flow structure is due to the streamlines being observed in the relative frame of reference with respect to the domain in question. The stationary inlet plenum shows that the introduced flow preferentially passes all of the radial passages and through the periodic surface, it is the holes immediately below the inflow that receive the most mass flow. Computation of the mass flow through each hole shows an order of magnitude difference between the highest and lowest. What is immediately apparent is the non-axisymmetric flow when turned into the axial direction and toward the rotating blocks.

In the rotating domain the flow is entering at a high level of incidence, causing a massive separation around the block. This leads to a high velocity jet for each passage travelling along the

pressure side. Occupying the majority of the passage width is a large streamwise vortex on the suction side of the block. A large 'puddle' of recirculating flow is seen on the outer radius although from this diagram the mechanisms of this flow structure are not apparent.
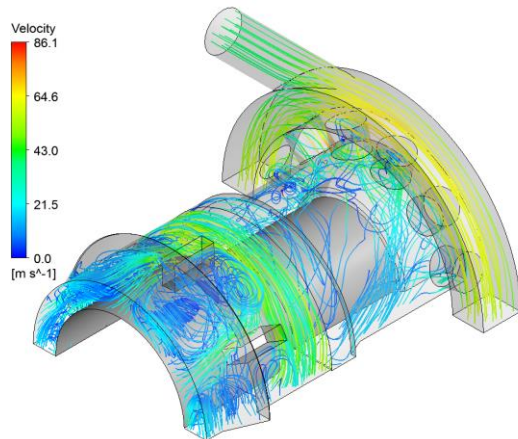
Figure 9: Velocity streamlines of final time-step. Colouring by flow velocity
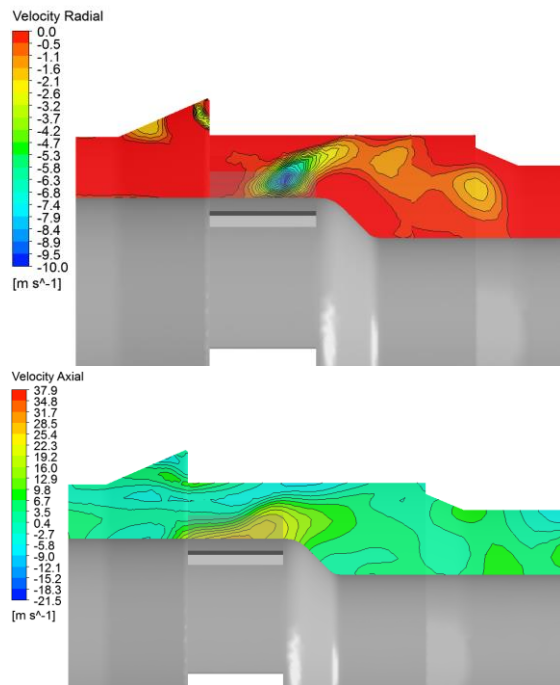
Figure 10: Negative radial velocity at mid-passage (a) and axial velocity at mid-passage (b).

Figures 10a and 10b show the radial and axial flow velocities respectively in the meridional plane. The outer labyrinth seal shown in Fig. 1 is seen at the outer radius on the right-hand side, downstream is the change in passage height ending immediately upstream of the block inlet. This region causes a separation in the flow field that distorts the block inlet, leading to the differing loading radially along the block; in turn this affects the flow upstream from the inlet. There is a strong radial migration from the outer radius inward along with an increasing axial velocity at the hub; this lifts the warm hub boundary layer. Although the effect is seen as strong it is only a low amount of mass flow affected. The recirculating puddle referred too earlier is displaced by more energetic flow, from these features the streamwise vortex is generated, this can be referred to as trailing shed vorticity, commonly known as a tip vortex on aircraft wings.
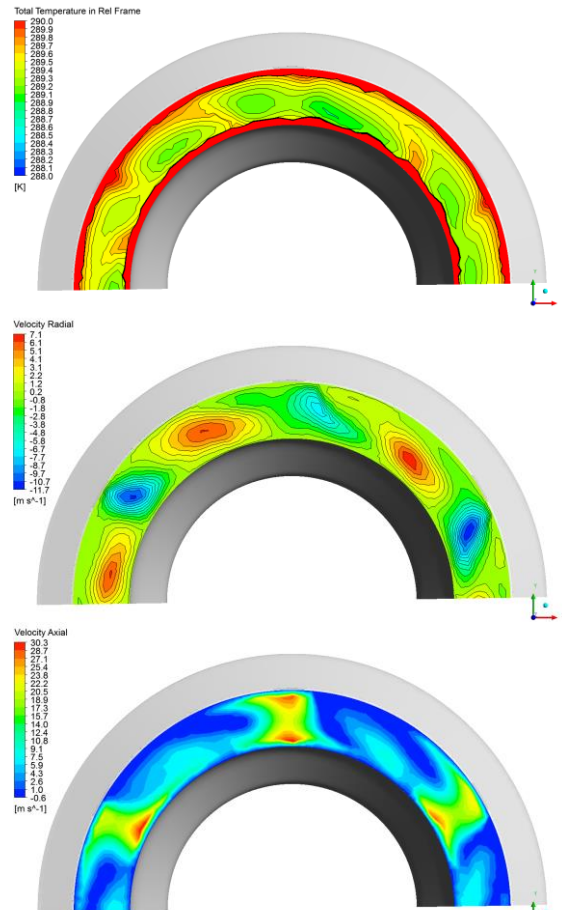
Figure 11: Relative total temperature at domain exit (a), radial velocity (b) and axial velocity (c).

The exit flow conditions can be seen in Figure 11 and can explain the profile of the shaft telemetry readings. Figures 11.b and 11.c clearly define the high momentum, predominantly axial jets off the block pressure side. The large blue regions (Fig 11.c) show the streamwise vortices with an axial core travelling approximately 1/3 of the jet speed. Either side of the vortex core the radial velocities show a clockwise rotation, with a warm region in radially outward components as show by Fig 11.a. The narrow contour range highlights the passage relative total temperature at the expensive of the showing the contours in the boundary layer. With the rotational velocity lower on the shaft surface than the outer radius, the vortex has time to increase in temperature on the shaft, which is present on the radially outward flow, shown by the

6

corresponding locations of high radial velocity and high passage temperature in Fig 11.a and 11.b.

The behaviour of the thermocouples can be explained by the radial and axial flow velocities, regardless of the relative rotational speed of the shaft and rotor. As shown in Fig. 4 the warming and cooling of the thermocouple bead have differing gradients. The warming is due to the streamwise vortex, which has a low axial velocity and lower temperature gradient. This is expected as the thermal response of a thermocouple bead is proportional to the Reynolds number and given the present flow conditions a strong function of the gas velocity. The converse is clear and the low temperature jet has a high axial velocity and a resultantly steep thermal gradient.

The space-time diagram of shown in Fig. 7 can now be re-interpreted with the numerical simulation. The high temperature streamwise vortex can be seen to persist the entire length of the test section whilst the low temperature jets tend to mix out. This is explained as vortices have been seen to persist through turbomachinery blade rows; the annulus of the MCR rig has no protrusions to disturb the vortex throughout the test section. The high momentum wakes (darker regions) are expected to move into the cavities and mix out quickly, highlighted by the darker regions in Fig 7. Further simulation is needed to confirm this and the effect the jets have on the structure of the cavity flow field and heat transfer.

The velocity of the thermal wakes can be compared to the CFD results of axial velocity, in the presented test run the axial velocity calculated from the mass flow rate is approximately 11.6 m/s. The flow velocity of the streamwise vortex can be estimated from the thermal peaks across the entire test section, giving an average of approximately 11.8m/s. A comparison to Figure 11.c and 11.a shows that the thermal hot spot has an axial velocity of approximately 10 m/s, giving a good agreement to the test data.

CONCLUSION

Low frequency telemetry has been used to capture thermal wakes propagating along the axial through-flow of the MCR during a high speed test. The test section rotational speed is of the order 8000 rpm, corresponding to approximately 133Hz whereas the recording frequency is 3Hz. Due to the relative rotation of two telemetry systems the thermal wakes can be captured when the relative speed is very low (of the order 3rpm), and can be seen to propagate along the entire test section.

Numerical analysis has been performed to give a first-order approximation of the flow field in a highly complex 3D domain. The profile of the thermal wakes is due to strong streamwise vorticities interspaced by high momentum, predominately axial jets. The vortices are shown to

be hotter than the jets due to the interaction with the shaft surface boundary layer. The profile of the thermal gradients between block passing are a function of the gas velocity, as this directly affects heat transfer to the thermocouple bead and in turn the thermal response.

This paper demonstrates a novel application of rotating, low frequency telemetry systems and since the data is not anti-aliased conclusive quantitate data regarding the phenomena cannot be stated. However the evidence does support the conjecture that the thermal profile is due to the blocks attached to the rotating assembly. Although not presented these wakes are a qualitative signature of the interaction of the axial flow field and multiple cavity setup and has shown variation under differing test conditions.

REFERENCES

Alexiou, A. *Flow and heat transfer in gas turbine HP compressor internal air systems.* DPhil Thesis, University of Sussex, UK: School of Engineering, 2000.

Atkins, N.R., Kanjirakkad, V. "Flow in a rotating cavity with axial throughflow at engine representative conditions." *ASME Turbo Expo.* Düsseldorf: ASME, 2014. GT2014-27174.

Long, C.A., Childs, P.R.N. "Shroud heat transfer measurements inside a heated multiple rotatingcavity with axial throughflow." *International Jounral of Heat and Fluid Flow* 28 (2007): 1405-1417.

Long, C.A., Miché, N.D.D., Childs, P.R.N. "Flow measurements inside a heated multiple rotatingcavity with axial throughflow." *International Journal of Heat anf Fluid Flow* 28 (2007): 1391-1404.

Miché, N.D. D. *Flow and heat transfer measurements inside a heated multiple rotating cavity with axial throughflow.* PhD Thesis, University of Sussex, UK: School of Engineering, 2008.

Owen, J.M., Long, C.A. "Review of Buoyancy-Induced flow in Rotating Cavities." *Jounral of Turbomachinery* 137 (2015): 111001-13.